

Analysis and Prediction of Size Effect on Laser Forming of Sheet Metal

Peng Cheng, Y. Lawrence Yao, Chao Liu, Duncan Pratt, and Yajun Fan, Dept. of Mechanical Engineering, Columbia University, New York, New York, USA

Abstract

Geometric effects play an important role in laser forming processes; however, few investigations have explored geometric effects other than those induced by sheet thickness. In this paper, the influence of component size or size effect, including variation of sheet width and sheet length, on laser-induced deformation is experimentally, numerically, and analytically investigated. An experimental matrix is designed to cover a wide range of sheet width and length for experiments and numerical simulation under different process conditions. Distinctive trends in bending angle are identified for varying sheet width, length, or both. The results are interpreted in terms of heat sink effect and bending nonuniformity. An analytical model is developed to facilitate size effect prediction. The model is based on the solution to a moving strip heat source over a finite size sheet. It also accounts for the pre-bending effect among consecutive segments on the scanning path. Analytical results are compared with an existing analytical model and numerical simulation.

Keywords: *Size Effect, Laser Forming, Analytical Model, Sheet Metal*

Introduction

Laser forming is a flexible manufacturing process that forms sheet metal by means of stresses induced by external heat instead of external force. It is a non-linear, thermomechanical process. Understanding various aspects of laser forming has been a challenging problem of considerable theoretical and practical interest. The relationships between bending distortion and process parameters, material properties, and workpiece thickness have been developed in analytical models. Additional information, such as influence of strain hardening, strain rate effects, and edge effect, has also been reported in experimental and numerical investigations.

The geometric effects in laser forming, however, have not been fully studied. Most research has

focused on the effect of workpiece thickness without considering other geometric attributes of the workpiece. Scully (1987) proposed that plate thickness, s_0 , is one of the primary factors in laser forming (two other primary factors are laser power, P , and scanning speed, V). Scully adopted a quantity, $P/(s_0\sqrt{V})$, that was used in arc welding to study the effect of plate thickness on bending angle, but he did not give an exact relationship between them. Koloman and Karol (1991) proposed an analytical model to express the relationship between bending angle and sheet thickness based on a pure energy approach. In this model, the bending angle is a function of the reciprocal of the square of thickness. However, the bending angles calculated from this formula are some orders of magnitude too large compared with experiments. Vollertsen proposed a simple, two-layer model based on the temperature gradient mechanism (TGM), with the temperature field obtained by an energy approach (Vollertsen 1994a) or by solving the 3-D heat conduction problem (Vollertsen 1994b). Both of Vollertsen's models have the same assumption that bending deformation is uniform along the sheet length so that the only geometric factor appearing in those models is plate thickness. Although more analytical models (Yau, Chan, and Lee 1997; Cheng and Lin 2001) were proposed recently and better agreements with the experimental results were reported, none of them have considered the effect of sheet size on laser forming deformation.

Experimental investigations and numerical simulation, however, have shown that sheet size has an effect on laser forming. Vollertsen (1994a) pointed out that the width of the sheet influences the cooling conditions and, therefore, the bending angle, and he also observed the influence of the sheet length on stress state. But he did not consider the size influences in his analytical solutions. Hsiao et al. (1997) found that for Inconel 625 the angular distortion

This paper is an expanded version of a paper presented at NAMRC 32 and published in the *Transactions of NAMRI/SME*, Vol. 32, 2004.

increases as sheet length increases, and he proposed that the reason is that the longer plate provides more cold metal to produce thermal stresses. He also proposed that there is an upper limit in the angular distortion with respect to the sheet length. However, these investigations on the influence of component size or size effect were empirical and did not lead to analytical prediction.

In this paper, the size effect exhibited in the laser forming process is investigated. First, the experimental and numerical investigations aimed at advancing the understanding of the causes of the size effect in straight-line laser forming are presented for a wide range of sheet sizes. Various deformation patterns due to the size effect are explained. To better quantify the role of size effect on laser forming, a predictive model is developed, in which finite sheet width and length are considered. The proposed model is experimentally validated.

Experiments and Simulation

Experiments of straight-line laser forming (Figure 1) were carried out following the matrix shown in Table 1, where the first number represents sheet length, L , and the second represents sheet width, W . In the present paper, the sheet length is defined as the dimension in the scanning direction and the sheet width is defined as the dimension perpendicular to the scanning direction. In this way, the size effect was investigated in three cases: varying sheet width, varying sheet length, and varying square size. Besides the listed sizes, additional sets of samples ($L = 20\sim 60$ mm, $W = 80$ mm) were used to further investigate the sheet length effect because it was reported (Vollertsen 1994a,b) that the effect of sheet length is more pronounced

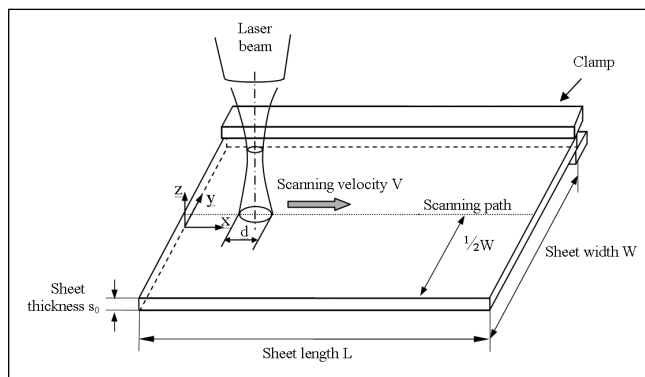


Figure 1
 Schematic of Straight-Line Laser Bending

when the length-to-thickness ratio (L / s_0) is small. The sheet thickness is fixed at 0.89 mm because the effect of thickness has been well studied and documented, as discussed in the previous section. Two sets of the experiments, with laser power 800 W, scanning velocity 50 mm/s and laser power 400 W, scanning velocity 25mm/s, were carried out. Although they involve the same line energy (P/V), the size effect on deformation may not be the same. The material investigated is cold-rolled AISI 1010 steel. The laser system used in the experiments is a PRC-1500 CO₂ laser, with a maximum output power of 1.5 kW and power density distribution of TEM₀₀. The diameter of the laser beam used is 4 mm, which is defined as the diameter at which the power density becomes $1 / e^2$ of the maximum power value. A coordinate measuring machine (CMM) is used to measure the bending angle. Bending angle may vary slightly along the scanning path, which is known as the edge effect (Bao and Yao 2001). Hence, bending angle was measured at five equally spaced locations along the scanning path and an average was calculated. To enhance laser absorption by the workpiece, graphite coating was applied to the surface exposed to the laser.

In numerical simulation, the laser forming process is modeled as a sequentially coupled thermal-mechanical process. In the thermal analysis, all the surfaces of the workpiece are subject to the convective heat flux, that is, $f = h(T - T_s)$, where h is the convective heat transfer coefficient, T is the surface temperature, and T_s is the surrounding temperature. The radiation heat flux is also considered at the heating surface, which is $f_c = \epsilon\sigma(T_4 - T_s^4)$, where ϵ and σ are emissivity and the Stefan-Boltzmann constant, respectively. More details can be found in Cheng and Yao (2003).

In the mechanical analysis, direct integration of the system is used for the nonlinear transient dynam-

Table 1
 Experiment Conditions for Size Effect
 (unit: mm; sheet size: Length \times Width ($L \times W$)
 below and throughout the paper)

Width	80	120	160	200
Length	80	120	160	200
80	80×80	80×120	80×160	80×200
120	120×80	120×120		
160	160×80		160×160	
200	200×80			200×200

ic response. The body force at a point can be expressed in the virtual work equation as

$$\int_V \mathbf{f} \cdot \delta \mathbf{v} dV = \int_V \mathbf{F} \cdot \delta \mathbf{v} dV - \int_V \rho \ddot{\mathbf{u}} \cdot \delta \mathbf{v} dV \quad (1)$$

where \mathbf{f} is the body force, $\delta \mathbf{v}$ is the “virtual” velocity field, V is the volume, \mathbf{F} is the externally prescribed force, ρ is the density of the material, and $\ddot{\mathbf{u}}$ is the acceleration field. With the nodal interpolation, the inertia force (d’Alembert force) is $-\left(\int_{V_0} \rho_0 \mathbf{N}^N \cdot \mathbf{N}^M dV_0\right) \ddot{\mathbf{u}}^M$; that is, the consistent mass matrix times the accelerations of the nodal variables, where \mathbf{N}^N or \mathbf{N}^M ($N, M = 1, 2, \dots$ up to the total number of variables in the problem) is a set of N vector interpolation functions (these are functions of the material coordinates), $\ddot{\mathbf{u}}^M$ is the nodal acceleration field, and ρ_0 and V_0 are the reference density and reference volume, respectively. Then, the equilibrium equation in numerical simulation is:

$$M^{NM} \ddot{\mathbf{u}}^M + I^N - P^N = 0 \quad (2)$$

where M^{NM} is the consistent mass matrix defined as

$$M^{NM} = \int_{V_0} \rho_0 \mathbf{N}^N \cdot \mathbf{N}^M dV_0 \quad (3)$$

I^N is the internal force defined as

$$I^N = \int_{V_0} \boldsymbol{\beta}^N : \boldsymbol{\sigma} dV_0 \quad (4)$$

where $\boldsymbol{\sigma}$ is stress, $\boldsymbol{\beta}^N$ is the matrix that defines the relation between strain variation and variations of the kinematic variables, $\delta \boldsymbol{\epsilon} = \boldsymbol{\beta}^N \delta \mathbf{v}^N$, and P^N is the external force vector defined as

$$P^N = \int_S \mathbf{N}^N \cdot \mathbf{t} dS + \int_V \mathbf{N}^N \cdot \mathbf{F} dV \quad (5)$$

where \mathbf{t} and \mathbf{F} are the external forces applied on the surface and body of material, respectively.

ABAQUS was used to complement the numerical simulation. A quadratic 20-node brick element was used in the mechanical analysis because this kind of element has no shear locking and hourglass stiffness and is also suitable for bending-deformation-dominated processes such as laser forming. To remain compatible with the structural analysis, an element type, DC3D20, is used in heat transfer analysis. A user subroutine of dflux was developed to model the heat source input from the Gaussian laser beam.

Experimental and Numerical Results with Discussions

Effect of Sheet Width

Figure 2 shows the variation of bending angle with sheet width while sheet length is kept constant. Good agreement has been obtained between the simulation and the experiment. Variation of the bending angle along the bending edge is due to the so-called edge effect (Bao and Yao 2001), which is also seen as the curved bending edge in Figure 3. It is seen from Figure 2 that, for low-carbon steel, when the sheet width increases, bending angle decreases. This differs from the observation on LF of Inconel 625 (Hsiao et al. 1997), where it was reported that bending angle increases with both sheet width and sheet length and it was attributed to larger thermal stress

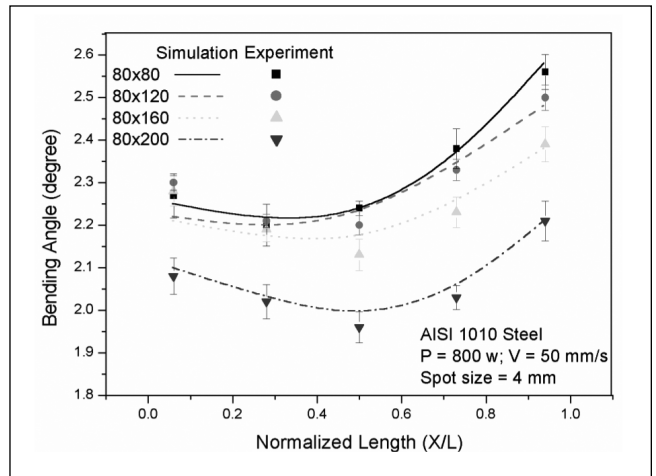


Figure 2
 Experimental and Numerical Results for Different Sheet Width

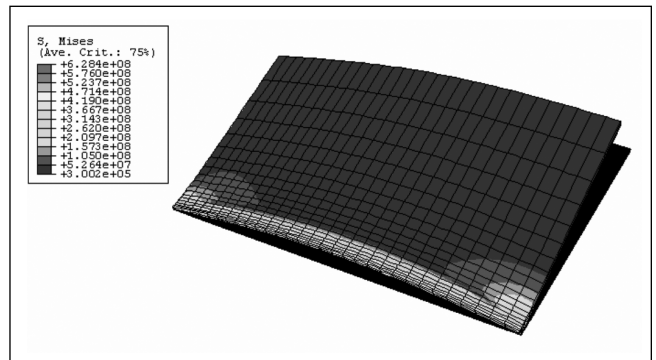


Figure 3
 Typical Simulation Result of Deformed Sheet Compared with Undeformed Sheet (deformation magnification 10X; half sheet of 80×80×0.89 mm, P = 800 W, V = 50 mm/s)

caused by larger constraint from the cold plate. The discrepancy is indicative that the size effect on bending angle may not be as simple as it was proposed.

When the sheet width varies, both heat dissipation and sheet weight vary. In numerical simulation, the weight effect was removed by deleting the gravity term in the model. *Figure 4* shows the bending angle difference between models with or without considering the gravity. It is found that, for the sheet width range investigated, the bending angle difference caused by gravity is almost the same for 80×80 and 80×200 samples, which clearly indicates that the gravity effect is not the major reason for the bending angle change caused by sheet width change. Further evidence was obtained by examining the Z-direction stress at a typical point 2 mm off the scanning path (*Figure 5*). It is seen that gravity

does not affect the bending stress significantly even as the sheet width increases from 80 to 200 mm. So, the reason of bending angle difference caused by different widths may lie in the thermal conduction condition.

Figure 6 shows the simulated time history of temperature. It is seen that the peak temperature at the top surface of the workpiece drops when the sheet width increases, while the temperature at the bottom surface is almost the same. The reduced temperature gradient in the thickness direction is clearly responsible for the reduced bending angle when sheet width increases. This is due to the fact that a larger width provides a larger heat sink. Difference of peak temperature between 80×80 and 80×200 sheets is almost 100K, which makes the average magnitude of bending angle differ by about 11 percent.

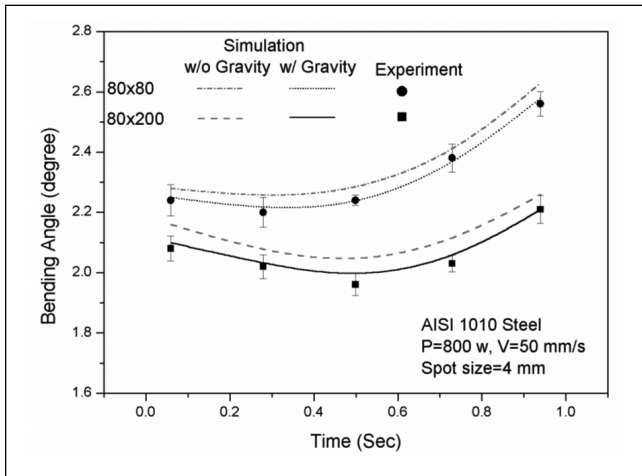


Figure 4

Influence of Gravity on Bending Angle when Sheet Width Varies

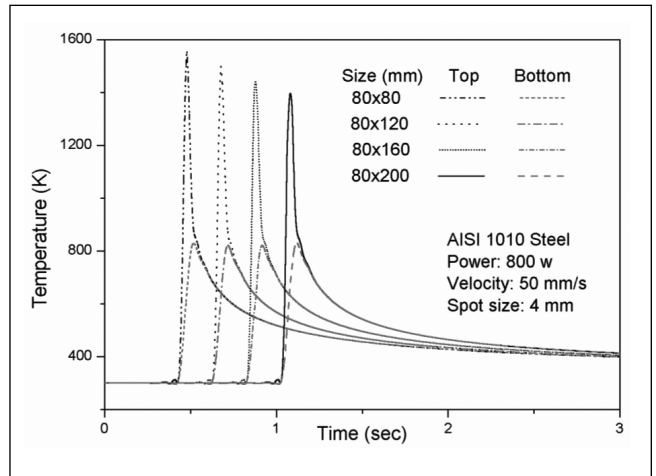


Figure 6

Simulated Time History of Temperature for Different Sheet Width (0.2 sec. time delay between each case for viewing clarity)

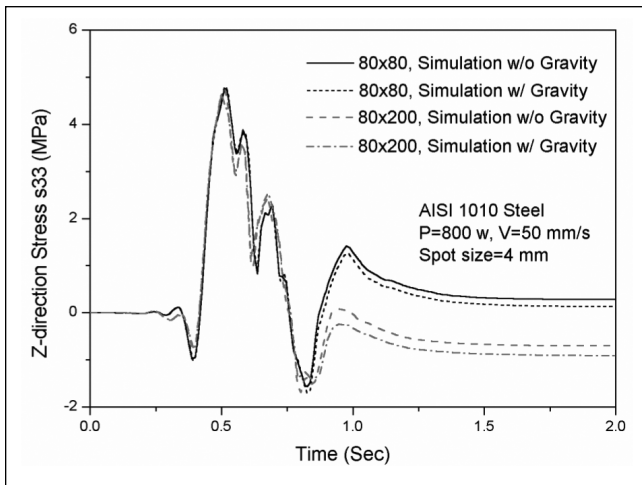


Figure 5

Simulation Results of Influence of Gravity on Bending Stress for Different Sheet Widths (at a typical point 2 mm off scanning path)

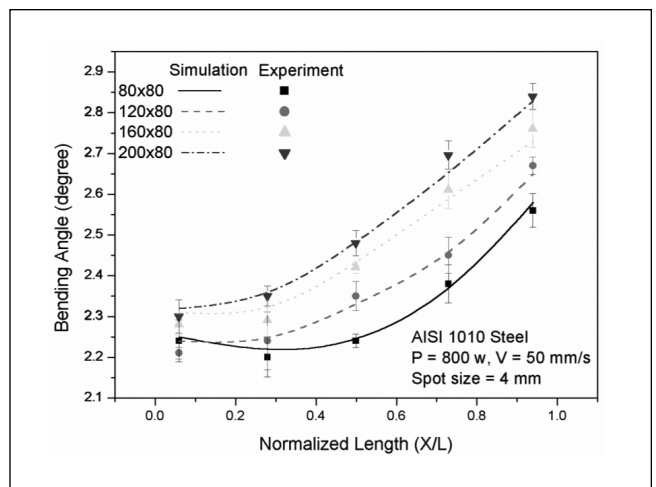


Figure 7

Experimental and Numerical Results for Different Sheet Length

Effect of Sheet Length

Figure 7 shows the variation of bending angle with sheet length while sheet width is kept constant. It is seen that, despite the fact that the laser power and scanning velocity are constant, the bending angle increases with sheet length. Figure 8 shows temperature on the top and bottom surfaces of work-piece. It is seen that, although the sheet length increases, the thermal field is not visibly affected. This is primarily because the heat sink effect discussed above is overshadowed in the direction of sheet length by the fast-moving laser beam along the same direction.

Figure 9 shows the time history of bending angle, peak temperature, and Z-direction stress in a 200x80 size sample at a typical position (x = 61.3 mm). It is

seen that before the laser beam reaches that point (signified by the rapid rise of temperature), the bending angle has reached about 1/3 of the final bending angle. When the laser beam reaches that point, the bending angle increases rapidly approximately until the Z-direction stress stabilizes. The bending angle continues to rise slowly after the laser passes. The existence of pre-bending and post-bending plays an important role in creating the final bending angle. Figure 10 compares the time history of the bending angle between 80x80 and 200x80 sheets at the same typical location (x = 61.3 mm). It is seen that there is more pre-bending effect in the shorter sheet (80x80) than in the longer sheet (200x80), and the opposite can be said about the post-bending effect. In any case, within the sheet length range investigated, the

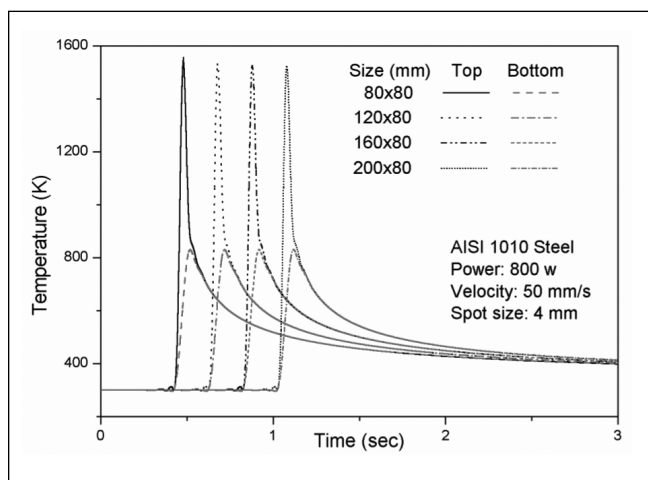


Figure 8

Simulated Time History of Temperature for Different Sheet Length (0.2 sec. time delay between each case for viewing clarity)

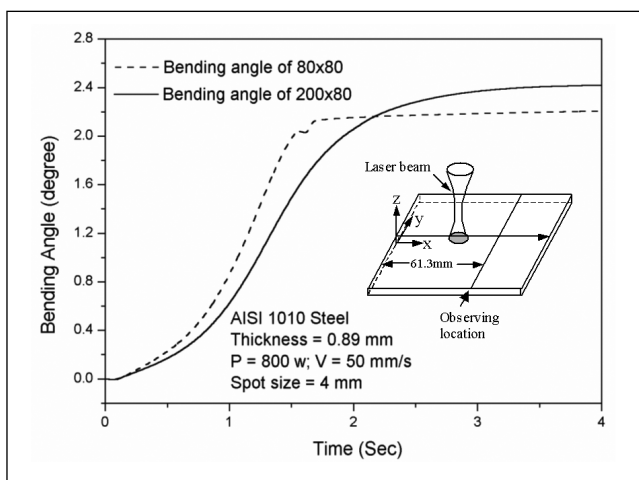


Figure 10

Comparison of Time History of Bending Angles Between Sheets of 80x80 mm and 200x80 mm

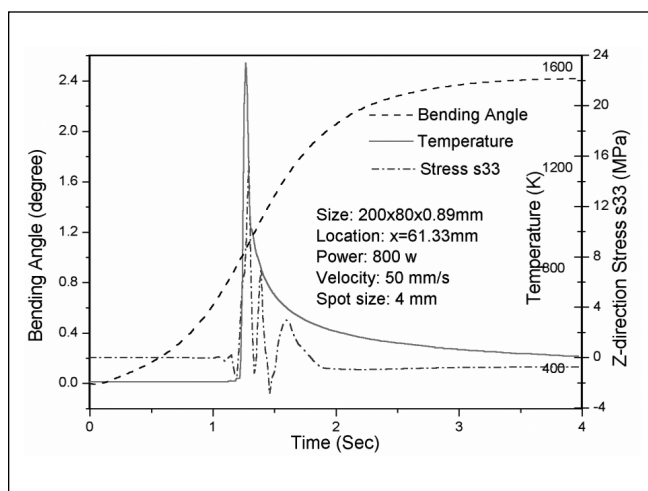


Figure 9

Simulated Time History of Bending Angle, Temperature, and Stress

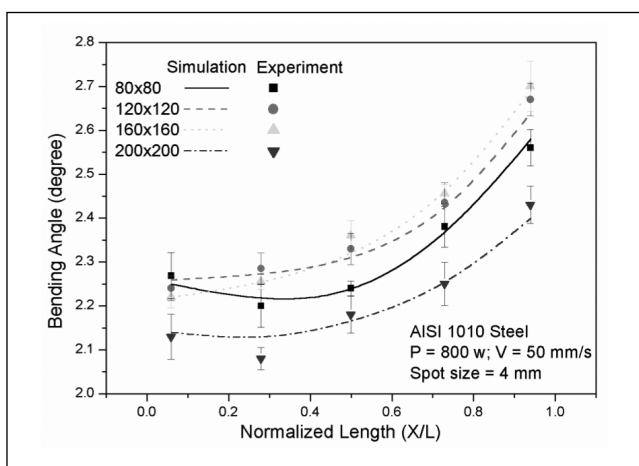


Figure 11

Experimental and Numerical Results when Sheet Length and Sheet Width Vary Proportionally

pre-bending effect is more significant than the post-bending effect. In a later section, the pre-bending effect is considered and incorporated in the development of an analytical model.

Varying Square Sizes

Figure 11 shows the bending angle trends when both sheet length and sheet width increase from 80 mm to 200 mm simultaneously. It is seen that the bending angle increases before it decreases. This is clearly because of the competing effects of heat sink and the pre-/post-bending effect. The pre-/post-bending effect is more dominant initially, and as a result the bending angle increases before the heat sink effect takes over and thus the bending angle decreases. Figures 12a and 12b show the

variation of average bending angle caused by size effects in 2-D and 3-D format, respectively. Figure 13 shows the size effect under the second condition ($P = 400 \text{ W}$, $V = 25 \text{ mm/s}$) and similar trends of size effects were found.

Inertial Effect

To investigate the size effect on bending angle, the inertial effect needs to be examined because it varies with sheet size. Figures 14 and 15 show the inertial effect on bending angle for varying sheet width and varying sheet length, respectively. It is clearly seen that the static model, in which the inertia effect is ignored, underestimates the bending angle. This is because the inertial force considered in the dynamic model makes the bending force larg-

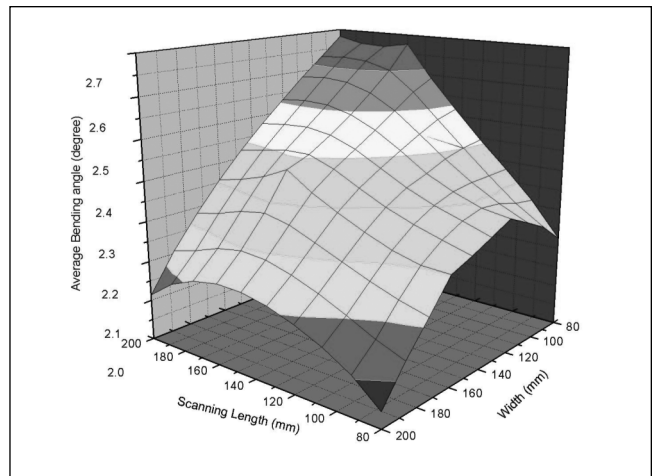
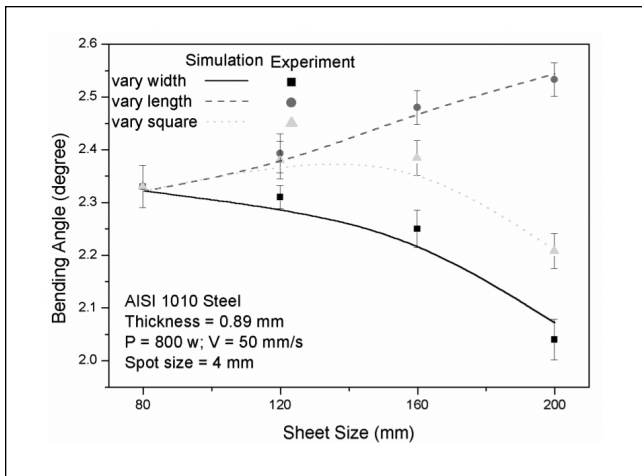


Figure 12
 Average Bending Angle Influenced by Sheet Size Effect ($P = 800 \text{ W}$, $V = 50 \text{ mm/s}$)
 (a) 2-D, and (b) 3-D plot

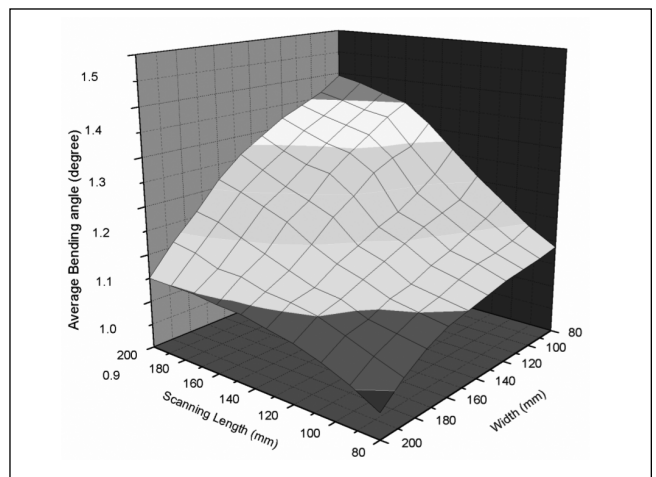
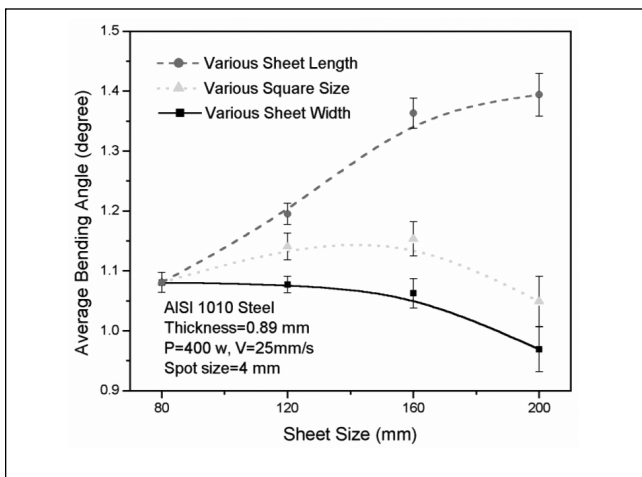


Figure 13
 Average Bending Angle Influenced by Sheet Size Effect ($P = 400 \text{ W}$, $V = 25 \text{ mm/s}$)
 (a) 2-D, and (b) 3-D plot

er and thus the bending angle larger than that of the static model. It is also seen that when sheet width increases (Figure 14), the bending angle difference between the dynamic and static model decreases. This is because the inertial force is mainly dependent on the difference between laser-induced thermal load and gravity. When the sheet width increases, the inertial force decreases due to the larger gravity and smaller thermal load caused by a larger heat sink effect (Figure 6). When sheet length increases (Figure 15), the inertial effect increases due to the more dominant thermal load due to the longer heat-input path.

Predictive Model Development

As mentioned before, laser forming is a nonlinear, thermomechanical process and is often simulated by a full three-dimensional finite element method. However, analytical models are more intuitive and depict the cause-effect relations directly. But considerable simplifications are required to succeed in developing such analytic models. The objective of this section is to develop an analytic model that can predict the size effect on bending angle by properly balancing between essential simplifications and model accuracy.

Existing Analytical Models and Proposed Approach

The most widely used model is perhaps the one developed by Vollertsen (1994a,b), which assumes the temperature gradient mechanism (TGM)

$$\alpha_B = \frac{3l_h \alpha_{th} \Delta T}{2s_0} \tag{6}$$

where α_B is the bending angle, l_h is the width of a heated zone, α_{th} is the thermal expansion coefficient, ΔT is the temperature rise in the heated zone, and s_0 is the sheet thickness. This model was arrived at by using a two-layer assumption, that is, the laser-induced temperature increase only occurs in the upper-half layer of the sheet. It also assumed that the thermal expansion caused by ΔT in the layer is fully converted into plastic compression and heat conduction can be neglected. As a result, the thermal field is obtained by an energy method

$$\Delta T = \frac{2AP}{Vc_p l_h s_0 \rho} \tag{7}$$

where A is the absorption coefficient, P is laser power, V is laser scanning velocity, c_p is heat capacity, and ρ is density. The bending angle prediction based on Eqs. (6) and (7) shows the same trends, but somewhat overestimates experimental measurements in most cases. Slightly improved models (Vollertsen and Rodle 1994; Yau, Chan, and Lee 1997) are also based on the same assumptions. The sheet size effect, however, is not incorporated. The bending angle is assumed to occur at once and, therefore, is uniform along the scanning path. In reality, α_B forms during and even before a laser beam reaches a point and is nonuniform along the scanning path, as seen from Figures 2 and 3.

To take into account heat conduction, Scully (1987) and Masubuchi (1992) adopted the solution

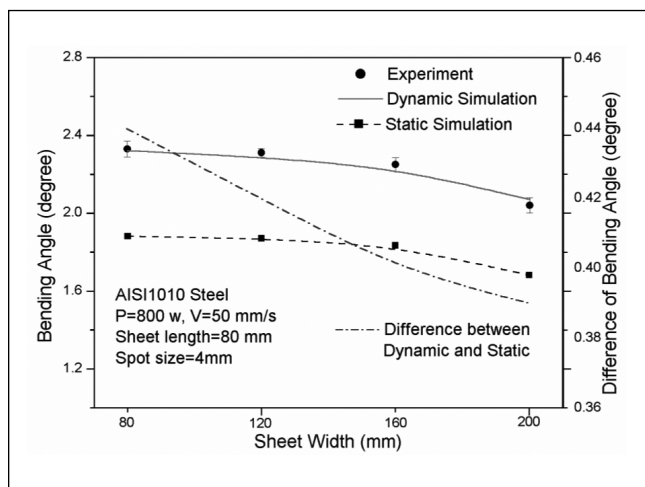


Figure 14
 Influence of Inertia Effect on Bending Angle
 when Sheet Width Varies from 80 mm to 200 mm

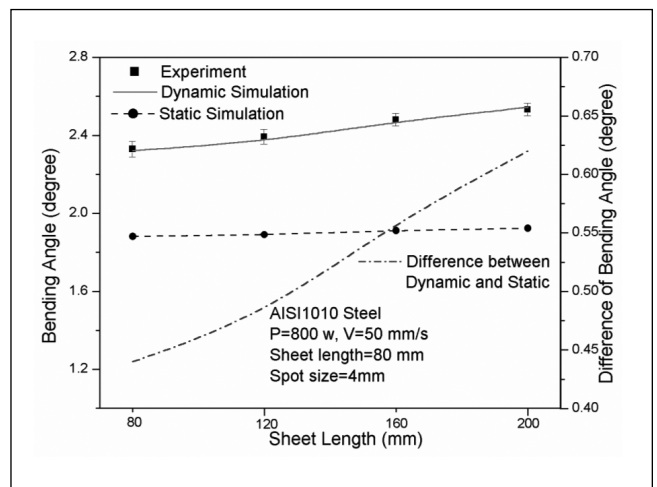


Figure 15
 Influence of Inertia Effect on Bending Angle
 when Sheet Length Varies from 80 mm to 200 mm

to the moving-line heat-source problem (Rosenthal 1947) to determine ΔT

$$\Delta T(r) = \frac{q}{\pi k g} e^{-\lambda V \xi} K_0(\lambda V r) \quad (8)$$

where q is the power of the line source, g is the height of the line source, k is the thermal conductivity, $\lambda = 1/2\kappa$ and κ is diffusivity, V is the moving speed along the x -axis, $\xi = x - vt$ is the distance to the heat source along the moving path, r is the distance to the source center in the scanning plane, and K_0 is the modified Bessel function of type zero. Equation (8) assumes uniform heating in the thickness direction and is appropriate for the upper layer in the two-layer model [Eqs. (6) and (7)] under TGM. Equation (8), however, is obtained based on a semi-infinite boundary condition and is not suitable for investigating the size effect.

As experimentally and numerically shown earlier, the sheet width effect on bending angle is primarily associated with the heat sink effect, while the sheet length effect is primarily associated with the pre-/post-bending effect. The proposed approach in this paper consists of (1) derivation of a ΔT expression for finite sheet width, W , taking into account the finite laser beam size; and (2) adaptation of Eq. (6) for a small segment of the scanning path (instead of the entire scanning path) and then derivation of an α_B expression for the scanning length, L .

Thermal Effect

The finite width condition is introduced in the solution of the moving-line heat source [Eq. (8)] by the method of images (Rosenthal 1947)

$$\Delta T = \frac{q}{\pi k g} e^{-\lambda V \xi} \sum_{n=-\infty}^{n=\infty} K_0(\lambda V r_n) \quad (9)$$

Taking into account the finite boundary condition, $\partial T / \partial y \rightarrow 0$ as $y = 0$ and $y = a = W/2$, a solution can be obtained by transforming Eq. (9) into a Fourier series. The obtained solution, however, is based on a line source without any line width, and the temperature value at the source center is infinite. To avoid this, an assumption that the line source has a finite width is made, and this assumption is realistic for the laser beam source. It is assumed that the moving line source has a width that equals the laser beam diameter on the sheet. By a series of derivations (see Appendix), the temperature within the line width, $-d/2 < \xi < d/2$, is

$$\Delta T = \frac{q}{\rho c_p a g V d} \left[\frac{1}{2\lambda V} + \left(\frac{d}{2} - \xi \right) \frac{e^{-2\lambda V(d/2+\xi)}}{2\lambda V} + \sum_{\mu_n(\mu_n+1)} \frac{2}{\mu_n(\mu_n+1)} \frac{1 - e^{-(\mu_n+1)\lambda V(d/2+\xi)}}{\lambda V} \cos \frac{n\pi y}{a} + \sum_{\mu_n(\mu_n-1)} \frac{2}{\mu_n(\mu_n-1)} \frac{1 - e^{(\mu_n-1)\lambda V(\xi-d/2)}}{\lambda V} \cos \frac{n\pi y}{a} \right] \quad (10)$$

where d is the laser spot size, g is the height of the line source (equal to half of the sheet thickness under the two-layer assumption), and $\mu_n = \sqrt{1 + \left(\frac{\pi n}{\lambda V a} \right)^2}$. Please note that ΔT is now a function of sheet width a . To obtain a representative ΔT for the two-layer model [Eq. (6)], the temperature increase in the square domain of d is averaged.

Figure 16a shows the temperature distribution of AISI 1010 steel sheet calculated by using the proposed analytical model. Because of the line heat source, it is interpreted as the temperature in the top layer of the two-layer model. It is seen that the isothermal lines are elliptic, similar to those for infinite sheet size, but in Figure 16a it has been possible to account for the heat sink effect primarily due to sheet width change. Figure 16b shows the temperature at the heat source center from the analytic model when sheet width varies. The decreasing trend with increasing sheet width is consistent with FEM simulation results, with some discrepancy in slope likely due to the several assumptions underlying the proposed analytic model, such as temperature-independent material properties and the two-layer assumption. Without considering the heat loss; infinity of the scanning length.

Mechanical Effect

As shown before, the sheet length effect on bending angle can be primarily accounted for through the pre-/post-bending effect along the scanning path. The pre-bending (bending at a location generated before the heat source arrives at the location) is more dominant than the post-bending (bending at a location generated after the heat source passes the location) in creating the final nonuniform bending angle. Therefore, only pre-bending is considered in the following derivation.

To consider the nonuniform bending along the scanning path, the scanning length, L , is divided into n segments. Each segment is L/n long and assumed to have a uniform bending along the segment

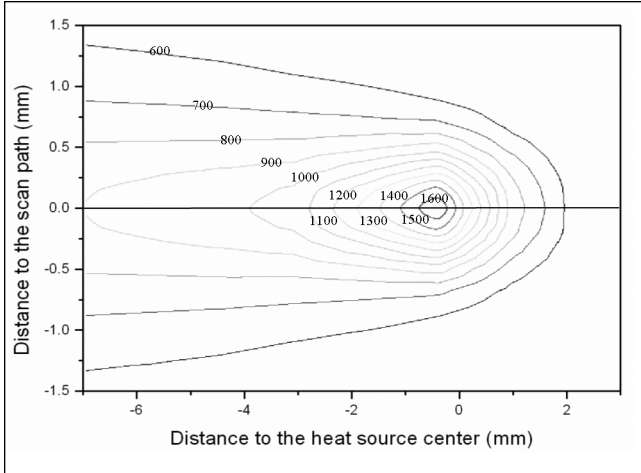


Figure 16a
Typical Temperature Distribution Calculated from Proposed Analytic Model for Finite Sheet Width (AISI 1010 steel, 80×80×0.89 mm, P = 800 W, V = 50 mm/s)

(Figure 17). For the segments that the heat source has passed, permanent plastic deformation occurs. For those segments where the heat source has not arrived, no plastic strain occurs and only the segment following the plastic-deformed segments is affected by the previous segment. Starting the analysis from the first segment, because there is no pre-bending effect the bending angle in the first segment, α_1 , can be obtained through a two-layer assumption (Vollertsen 1994a), that is

$$\alpha_1 = \frac{2l_h (\epsilon_{low} - \epsilon_{up})}{s_0} \quad (11)$$

where ϵ_{up} and ϵ_{low} are strains of the upper and lower layer, respectively. Assuming that the thermal expansion is fully converted into the plastic compression, one obtains

$$\epsilon_{up} = \epsilon_{el} + \epsilon_{pl} = \left(\frac{F}{EA} - \frac{M s_0}{EI} \right) + (-\alpha_{th} \Delta T) \quad (12)$$

$$\epsilon_{low} = -\epsilon_{el} = -\frac{F}{EA} + \frac{M s_0}{EI} \quad (13)$$

where F and M are the force and moment, respectively, generated by the difference in compression between the upper and lower layer of the segment, E is the elastic modulus, A is the cross-sectional area (x - z plane) of each layer of the segment given by $A = \frac{1}{2} s_0 \frac{L}{n}$, and I is the inertia momentum given by $I = \frac{1}{12} \frac{L}{n} s_0^3$. Substituting

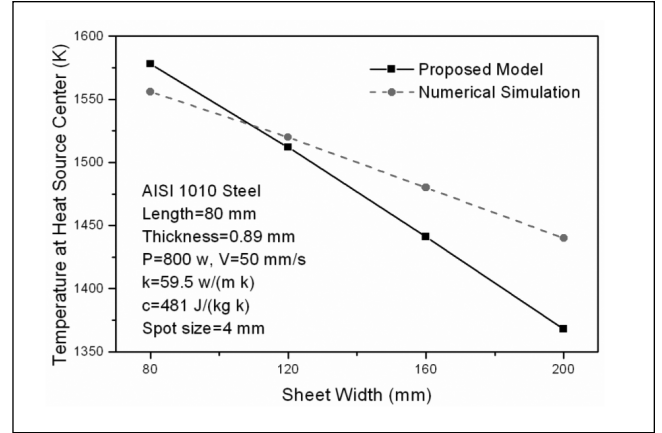


Figure 16b
Comparison of Temperature Between Proposed Analytic Model for Finite Sheet Width and FEM Simulation (at heat-source center)

Eqs. (12) and (13) into Eq. (10) and noting the equilibrium equation, $F \cdot \frac{s_0}{2} = M = \frac{EI}{l_h} \alpha_1$, it is obtained that

$$\alpha_1 = \frac{3l_h \alpha_{th} \Delta T}{2s_0} \equiv \alpha \quad (14)$$

and

$$\epsilon_{el} = -\frac{1}{4} \alpha_{th} \Delta T \quad (15)$$

For the second segment, although the heat source has not reached it, elastic strain will still occur so as to be compatible with the first segment. The elastic strain at the boundary between the first and the second segment is equal to the elastic strain of the first segment. The elastic strain at the boundary between the second and the third segment is zero. The average elastic strain in the second segment is

$$\bar{\epsilon}_{up} = \frac{1}{2} \epsilon_{el} = -\frac{1}{8} \alpha_{th} \Delta T \quad \text{and} \quad \bar{\epsilon}_{low} = \frac{1}{2} \epsilon_{el} = -\frac{1}{8} \alpha_{th} \Delta T \quad (16)$$

Then the equivalent elastic forces on the upper and lower layer of the second segment are

$$\bar{P}_{up} = EA \bar{\epsilon}_{up} = -\bar{P}_{low} \quad (17)$$

It can be assumed that the forces are loaded at the center point of each applied plane. Then the pre-bending angle of the second segment can be obtained:

$$\Delta \alpha_1 = \frac{P_{up} \cdot \frac{1}{2} s_0}{EI} l_h = \frac{3}{8} \frac{l_h}{s_0} \alpha_{th} \Delta T = \frac{1}{4} \alpha_1 \quad (18)$$

The final bending angle of the second segment is equal to the summation of the bending angle caused by heat flux and the pre-bending angle:

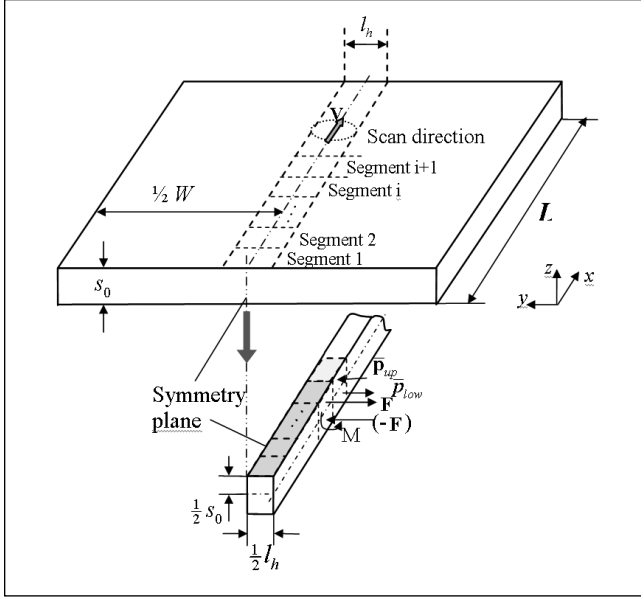


Figure 17
Schematic of Mechanical Model
(forces assumed to be applied at center of relevant surface)

$$\alpha_2 = \alpha + \frac{1}{4} \alpha_1 \quad (19)$$

Similarly, when the heat source moves out of the second segment and has not entered the third segment, the pre-bending angle of the third segment is $\frac{1}{4}\alpha_2$. In general, the bending angle of the i -th segment is

$$\alpha_i = \alpha + \frac{1}{4} \alpha_{i-1} \quad (20)$$

where α_{i-1} is the bending angle of the $(i-1)$ th segment.

Then, the average bending angle of a plate with the length of L and consisting of n segments is

$$\bar{\alpha} = \frac{4}{3} \left[1 - \frac{1}{3n} \left(1 - \frac{1}{4^n} \right) \right] \alpha \approx \frac{4}{3} \left(1 - \frac{1}{3n} \right) \alpha \quad (21)$$

Substituting the expression of α shown in Eq. (14) into Eq. (21) obtains

$$\bar{\alpha} = \left(1 - \frac{1}{3n} \right) \frac{2l_h}{s_0} \alpha_{th} \Delta T \quad (22)$$

where the temperature increment, ΔT , can be obtained by the thermal model introduced in the previous section. Equation (22) predicts the bending angle of a finite-sized sheet. The effect of sheet width is reflected in ΔT , and the effect of sheet length is

reflected in n . To apply Eq. (22) to a specific laser forming process involving a specific material, n and l_h need to be determined; both are related to the extent of the plastically deformed zone. Vollertsen and Rodle (1994) have derived an expression for l_h based on a fixed-point source and infinite boundary conditions. Though many simplifications have been taken, the solution is still so complex that it is not convenient to be applied into analytical models. Yau, Chan, and Lee (1997) took the beam spot size, d , as l_h in their analytical model, which makes the expression succinct, but it is not exact.

The temperature above which significant plastic strain occurs is termed critical temperature (Vollertsen 1994a; Yu 2000). By the stress-strain curve of low-carbon steel sheet, it is found that the plastic state starts when the engineering strain is larger than ~ 0.5 percent, and the corresponding critical temperature can be approximately obtained by $\varepsilon = \alpha_{th} \Delta T$ and is around 700 K (Figure 18). Using temperature distributions predicted by the proposed thermal model (see previous section) under various conditions, the range of the plastic-deformed zone in which the temperature is higher than critical temperature (~ 700 K) is approximately determined and related to the line energy, P/V (Figures 19a and 19b) as

$$l_h \approx 0.125(P/V) + 0.5 \quad (23)$$

$$l_h \approx 0.125(P/V) + 0.5 \quad (24)$$

In above equations, the units of length, power, and velocity are mm, watt, and mm/s, respectively. Substituting Eqs. (23) and (24) into Eq. (22), one can predict the bending angle of a finite-sized sheet.

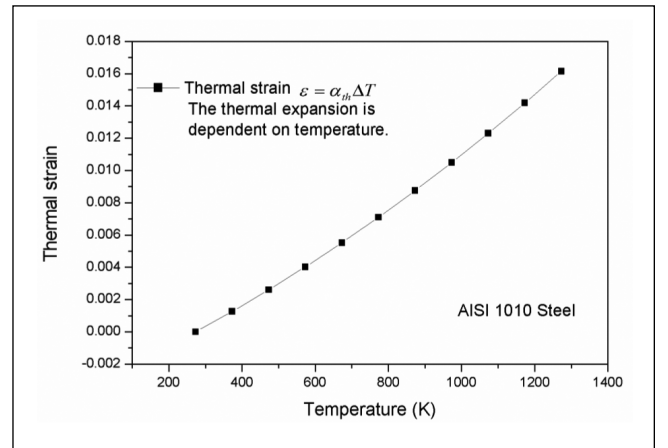


Figure 18
Calculated Thermal Strain Corresponding to Temperature-Dependent Thermal Expansion Coefficients of Low-Carbon Steel

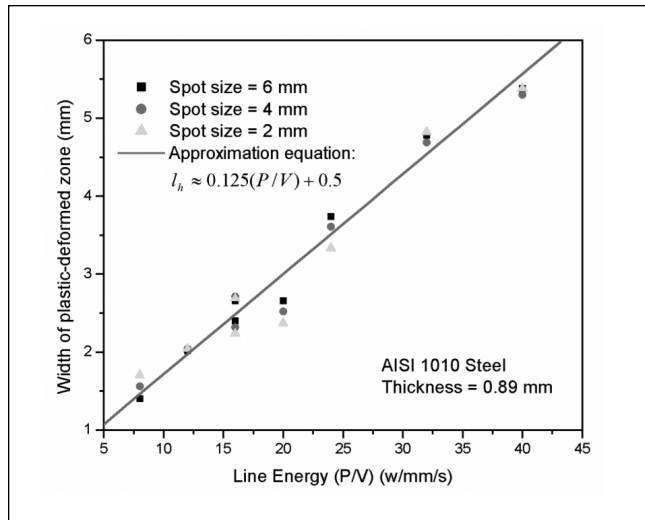


Figure 19a
 Width of Plastic-Deformed Zone vs. Line Energy
 by Proposed Thermal Model

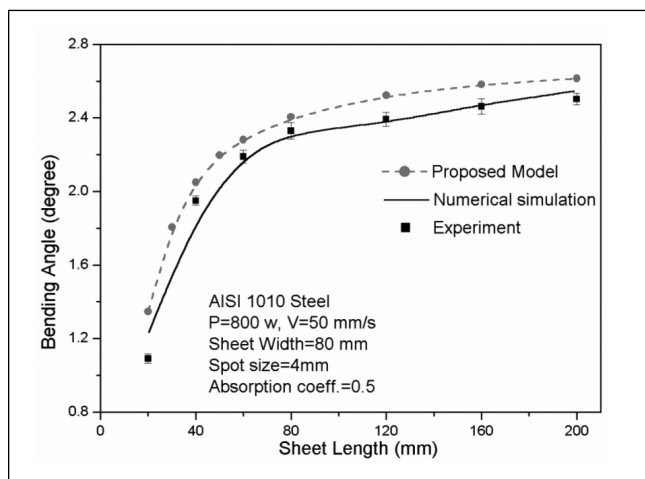


Figure 19b
 Length of Plastic-Deformed Zone vs. Line Energy
 by Proposed Thermal Model

Validation of Predictive Model

Figures 20 to 22 show the comparison of values obtained by the proposed model and experiments, numerical simulation, and an existing analytical model (Vollertsen 1994a). It is seen that the bending angle values obtained from the proposed model show a similar trend to the experiments and numerical simulation. This can be compared to the existing analytic model, which is unable to predict the size effect. The agreement of the proposed model with experimental and simulation values is significantly better compared with the other analytical model. In the case of varying sheet length (Figure 21), the model-predicted trend of bending angle is well

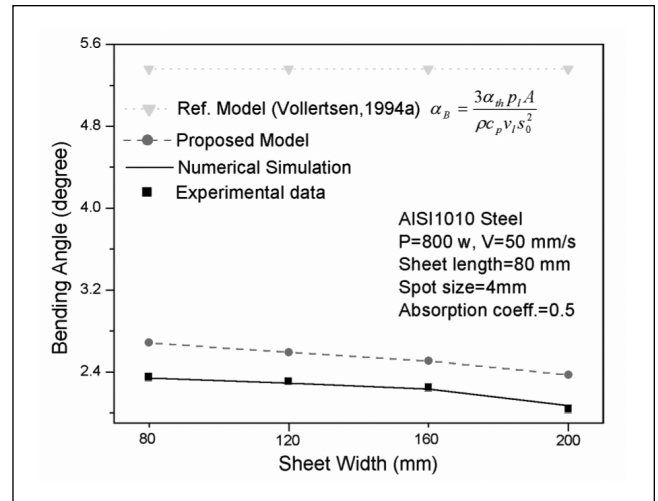


Figure 20
 Analytic Prediction of Bending Angle for Varying Sheet Width

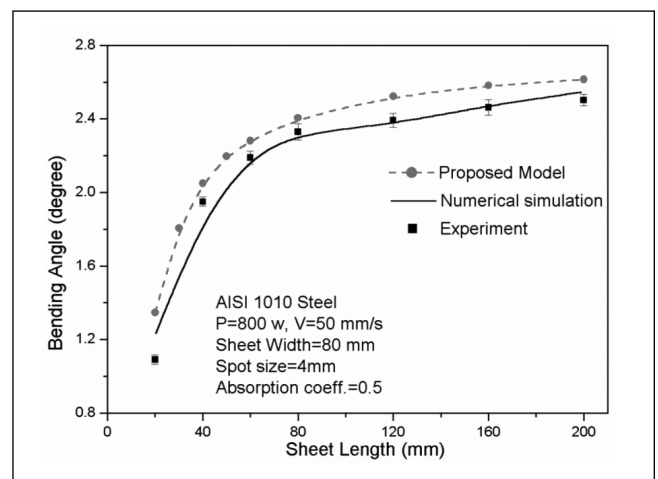


Figure 21
 Analytic Prediction of Bending Angle for Varying Sheet Length

agreeable with the experimental and simulation values. The trend is consistent with Vollertsen's (1994a) experimental observations; that is, when the ratio of length and thickness is small, the increasing trend of bending angle with sheet length is more pronounced and there is an upper limit of bending angle when the sheet length keeps increasing. In the comparison of varying square size (Figure 22), the predictive model also captures the variation trend. It should be noted that the comparison of bending angle of the 40×40 mm sheet is only between a predicted value and a simulated value.

The predictive model is also validated under another condition ($P = 400$ W, $V = 25$ mm/s). The comparison between proposed model, experiment, and existing model is shown in Figure 23. Although

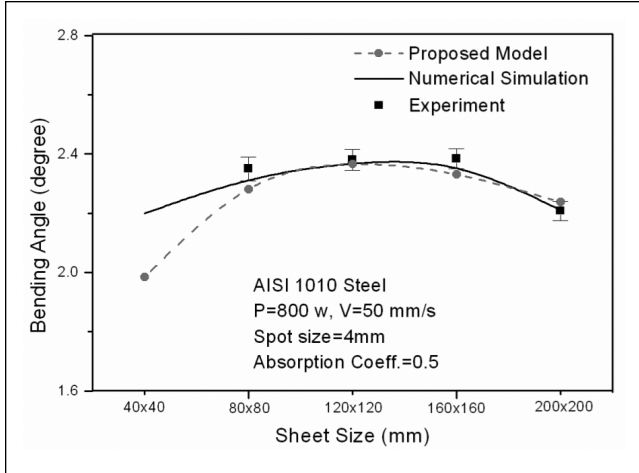


Figure 22

Analytic Predictions of Bending Angles for Varying Square Sheet Size

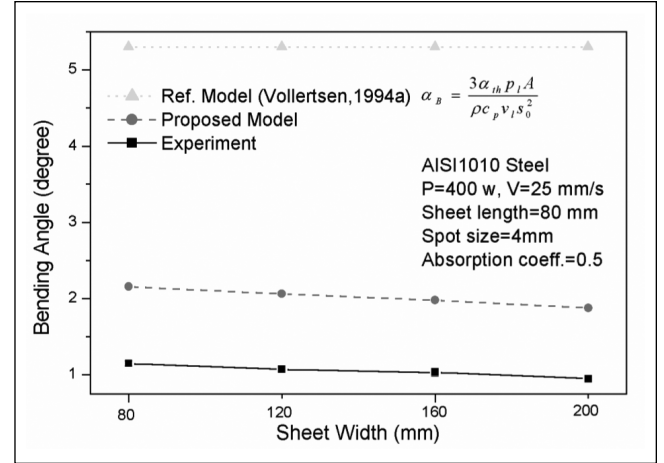


Figure 23

Prediction of Bending Angles for Varying Sheet Width
($P = 400 \text{ W}$, $V = 25 \text{ mm/s}$)

the proposed model can predict the trend of bending angles, the discrepancy is larger than that under the first condition ($P = 800 \text{ W}$ and $V = 50 \text{ mm/s}$). Because of the lower input energy and larger time for heat dissipation under this condition, the temperature gradient is not as steep as under the first condition. As a result, the two-layer assumption is less valid under this condition. But the proposed model is still much closer to the experimental values than the existing model.

Conclusions

Size effect is important for the quality control of the products produced by laser forming. To better understand the deformation characteristics and provide a useful tool to predict the bending deformation of plates with different sheet sizes, the size effect on laser forming of low-carbon steel sheet has been investigated. The bending angle decreases when sheet length is constant and sheet width increases. This is primarily due to the increased heat sink effect with increasing sheet width. The bending angle increases when sheet width is constant and sheet length increases. This is primarily due to the fact that the bending angle along the scanning path is nonuniform and influenced by the pre/post-bending effect. When both the sheet length and sheet width increase in even proportion, the bending angle increases before decreasing due to the competing effects. Based on the experimental and numerical results and physical interpretations above, an analytical model has been developed to predict the size effect. The effect of sheet width is accounted for by modeling a

moving “strip” heat source over a finite-width sheet. The effect of sheet length is modeled by dividing a finite scanning path into small segments and taking into account the pre-bending effect between consecutive segments. The predictive model compares favorably with the existing analytical model in terms of agreement with experimental measurement and numerical simulation.

Appendix

The temperature field for a moving-line heat source (along the x -direction in speed V) in a plate of finite width a and infinite length was presented in Rosenthal’s classic paper (1947)

$$\Delta T = \frac{q}{c_p \rho a g V} \left[\exp(-2\lambda V \xi) + \sum_{n=1}^{\infty} \frac{2}{\mu_n} \exp[-(\mu_n + 1)\lambda V \xi] \cos \frac{\pi n y}{a} \right] \text{ for } \xi > 0 \quad (\text{A1})$$

$$\Delta T = \frac{q}{c_p \rho a g V} \left[1 + \sum_{n=1}^{\infty} \frac{2}{\mu_n} \exp[(\mu_n - 1)\lambda V \xi] \cos \frac{\pi n y}{a} \right] \text{ for } \xi < 0 \quad (\text{A2})$$

where q is input power per unit time, g is the height of heat source, $\lambda = 1/2\kappa$ and κ is the diffusivity, $\xi = x - vt$ is the distance to the heat source along the moving path, and

$$\mu_n = \sqrt{1 + \left(\frac{\pi n}{\lambda V a} \right)^2} \quad (\text{A3})$$

The inconvenience of above equation is that temperature is infinite at the location of the source,

which is not true for a laser heat source. To be suitable for a laser forming process, a moving-strip heat source instead of a single line is assumed to spread over a certain area. The heat source is represented as being composed of an infinite number of infinitely small linear sources, $q''d\xi'$, set side by side from $\xi' = -d/2$ to $\xi' = d/2$, where d is the beam spot size. q'' the rate of heat per unit area and $q''d\xi' = \frac{q}{gd}d\xi'$, where g is the height of the line source (equal to half of the sheet thickness under the two-layer assumption). According to Eqs. (A1) and (A2), a linear source of strength $\frac{q}{gd}d\xi'$ placed at a distance ξ' from the origin contributes to the temperature of a point ξ, y in the amount of

$$\Delta T = \frac{qd\xi'}{c_p \rho a g V d} \left[e^{-2\lambda V(\xi-\xi')} + \sum_{n=1}^{\infty} \frac{2}{\mu_n} e^{-(\mu_n+1)\lambda V(\xi-\xi')} \cos \frac{\pi n y}{a} \right] \text{ for (A4)}$$

$$\Delta T = \frac{qd\xi'}{c_p \rho a g V d} \left[1 + \sum_{n=1}^{\infty} \frac{2}{\mu_n} e^{(\mu_n-1)\lambda V(\xi-\xi')} \cos \frac{\pi n y}{a} \right] \text{ for (A5)}$$

The temperature increase can be obtained by integrating Eqs. (A4) and (A5) in the domain of $\xi > d/2$, $\xi < -d/2$, and $-d/2 < \xi < d/2$, respectively. Then, three cases may be distinguished according to whether the point (ξ, y) is located outside or inside the portion of the sheet covered by the strip source.

For $\xi > d/2$, integrating Eq. (A4) from $\xi' = -d/2$ to $\xi' = d/2$ gives

$$\Delta T = \frac{q}{\rho c_p a g V d} \left[\frac{e^{-2\lambda V \xi}}{2\lambda V} (e^{-\lambda V l_h} + e^{\lambda V l_h}) + \sum_{n=1}^{\infty} \frac{2}{\mu_n(\mu_n+1)} \cdot \frac{e^{-(\mu_n+1)\lambda V \xi}}{\lambda V} \left(e^{\left(\frac{\mu_n+1}{2}\right)\lambda V l_h} - e^{-\left(\frac{\mu_n-1}{2}\right)\lambda V l_h} \right) \cos \frac{\pi n y}{a} \right] \text{ (A6)}$$

For $\xi < -d/2$, integrating Eq. (A5) from $\xi' = -d/2$ to $\xi' = d/2$ gives

$$\Delta T = \frac{q}{\rho c_p a g V d} \left[d + \sum_{n=1}^{\infty} \frac{2}{\mu_n(\mu_n-1)} \cdot \frac{e^{(\mu_n-1)\lambda V \xi}}{\lambda V} \left(e^{\left(\frac{\mu_n+1}{2}\right)\lambda V l_h} - e^{-\left(\frac{\mu_n-1}{2}\right)\lambda V l_h} \right) \cos \frac{\pi n y}{a} \right] \text{ (A7)}$$

For $-d/2 < \xi < d/2$, integrating Eq. (A4) in $-d/2 < \xi' < \xi$, integrating Eq. (A5) in $\xi < \xi' < l_h/2$, and then adding them obtains the temperature field shown as Eq. (10) in the text. The temperature increment at the center of the heat source ($\xi = 0, y = 0$) is given by

$$\Delta T = \frac{A p_l}{4 \rho c_p a g V} \left\{ 1 + \frac{1}{\lambda V d} \left[1 - \exp(-\lambda V d) + \frac{4}{\lambda V d} f(\mu_n, \lambda V d) \right] \right\} \text{ (A8)}$$

where

$$f(\mu_n, \lambda V d) = \sum_{n=1}^{\infty} \frac{1}{\mu_n(\mu_n+1)} \left\{ 1 - \exp[-\lambda V d(\mu_n+1)/2] \right\} + \sum_{n=1}^{\infty} \frac{1}{\mu_n(\mu_n-1)} \left\{ 1 - \exp[-\lambda V d(\mu_n-1)/2] \right\} \text{ (A9)}$$

References

- Bao, J. and Yao, Y.L. (2001). "Analysis and prediction of edge effects in laser bending." *Journal of Mfg. Science and Engg.* (v123), pp53-61.
- Cheng, P.J. and Lin, S.C. (2001). "An analytical model to estimate angle formed by laser." *Journal of Materials Processing Technology* (v108), pp314-319.
- Cheng, P. and Yao, Y.L. (2003). "The influence of sheet metal anisotropy on laser forming process." *Proc. of ICALEO'03*, Section E, pp1-10.
- Hsiao, Y.C.; Shimizu, H.; Firth, L.; Maher, W.; and Masubuchi, K. (1997). "Finite element modeling of laser forming." *Proc. of ICALEO'97*, Section A, pp31-40.
- Koloman, K. and Kraol, P. (1991). "Formen durch locale Erwärmung." *Metal Forming - Theory and Practice: Proc. of 5th Int'l Conf. on Metal Forming*, M. Tisza and K. Kardos, eds., pp69-75.
- Li, W. and Yao, Y.L. (2000). "Numerical and experimental study of strain rate effects in laser forming." *Journal of Mfg. Science and Engg.* (v122), pp445-451.
- Masubuchi, K. (1992). "Studies at MIT related to applications of laser technologies to metal fabrication." *Proc. of LAMP'92*, pp939-946.
- Rosenthal, D. (1947). "The theory of moving sources of heat and its applications to metal treatments." *Trans. of ASME, Journal of Heat Transfer* (v68), pp849-866.
- Scully, K. (1987). "Laser line heating." *Journal of Ship Production* (v3, n4), pp237-246.
- Vollertsen, F. (1994a). "An analytical model for laser bending." *Lasers in Engg.* (v2), pp261-276.
- Vollertsen, F. (1994b). "Mechanisms and models for laser forming." *Laser Assisted Net Shape Engg., Proc. of LANE'94* (v1). Meisenbach Bamberg, pp345-360.

- Vollertsen, F. and Rodle, M. (1994). "Model for the temperature gradient mechanism of laser bending." *Laser Assisted Net Shape Engg., Proc. of LANE '94* (v1). Meisenbach Bamberg, pp371-378.
- Yau, C.L.; Chan, K.C.; and Lee, W.B. (1997). "A new analytical model for laser bending." *Laser Assisted Net Shape Engg., Proc. of LANE '97* (v2). Meisenbach Bamberg, pp357-366.
- Yu, G. (2000). "Modeling of shell forming by line heating." Doctoral thesis. Cambridge, MA: Massachusetts Institute of Technology, pp56-69.

Authors' Biographies

Peng Cheng is a PhD candidate in the Dept. of Mechanical Engineering at Columbia University. He received a BS in 1997 and MS in 2000 in mechanical engineering from Tsinghua University, China. His research interest is laser forming.

Y. Lawrence Yao is a professor in the Dept. of Mechanical Engineering at Columbia University. He received his PhD from the University of Wisconsin-Madison in 1988. He is interested in multidisciplinary research in manufacturing and design, nontraditional manufacturing processes, and laser materials processing.

Chao Liu was a graduate student in the Dept. of Mechanical Engineering at Columbia University. He received a master's degree in 2003. His research interest is laser forming.

Duncan Pratt was an undergraduate in the Dept. of Mechanical Engineering at Columbia University. He received a BS in 2004. He is currently working at the GE Global Research Center.

Yajun Fan is a PhD student in the Dept. of Mechanical Engineering at Columbia University. He received an MS in materials science from Pennsylvania State University in 2003. His current research is on laser material processing.